NASA

Technical Memorandum 84962

The Radiative Impact of Cumulus Cloudiness in a General Circulation Model

Chin-Hoh Moeng and David A. Randall

December 1982

Laboratory for Atmospheric Sciences
Modeling and Simulation Facility

National Aeronautics and
Space Administration

Goddard Space Flight Center
Greenbelt, Maryland 20771

THE RADIATIVE IMPACT OF CUMULUS CLOUDINESS IN A GENERAL CIRCULATION MODEL

Chin-Hoh Moeng

Sigma Data Services, Corp.
Laboratory for Atmospheric Sciences
NASA/Goddard Space Flight Center
Greenbelt, MD 20771

and

David A. Randall

Laboratory for Atmospheric Sciences
NASA/Goddard Space Flight Center
Greenbelt, MD 20771

Abstract

Cumulus clouds are observed to produce a very small fractional cloudiness, yet in the GLAS climate model they are assumed to fill an entire grid area (~500 km x 400 km). To study the effect of such excessive cumulus cloudiness on the radiational heating and, consequently, on other aspects of the model climatology, we have performed an experiment, for a July simulation, in which the cumulus cloudiness is neglected completely for purposes of the solar and terrestrial radiation parameterizations. The results are compared with those of a control run, in which 100% cumulus cloud cover is assumed.

The net solar radiation input into the earth-atmosphere system is more realistic in the experiment, and the model's underprediction (by about 40 W m^{-2}) of the global-mean outgoing thermal radiation at the top of the atmosphere is somewhat reduced.

Comparison of the experiment and control suggests that there exists a positive feedback between cumulus convection and the radiation field. Treating the cumulus clouds as having zero cloudiness produces fewer deep cumulus clouds; apparently, the radiative effects of cumulus clouds tend to favor further convective activity.

The upper troposphere is warmer in the experiment, especially in the middle latitudes of the Northern (summer) Hemisphere. The vertical shear of the zonal wind is correspondingly reduced. The surface air temperature increases over land, and the thermal lows over the continents intensify.

The precipitation maximum over the tropical oceans shifts southward in the experiment.

1. Introduction

A number of cloud-radiation studies have previously been made with the GLAS (Goddard Laboratory for Atmospheric Sciences) climate model (Herman et al., 1980; Shukla and Sud, 1981); these studies were reviewed by Herman (1980). In a "transparent cloud" experiment, Herman et al. (1980) eliminated the cloud interactions first with solar radiation and then with terrestrial radiation. They concluded that the treatment of all clouds as transparent to the radiation stream increases the global-mean radiative flux into the top of the atmosphere by 16 W m^{-2}. In a "fixed cloud" experiment (Shukla and Sud, 1981), the spatial distribution of clouds was computed once and fixed in time. The results showed that a fixed cloud distribution acts as a zonally asymmetric, stationary thermal forcing, and produces a significant change in the large-scale dynamical circulation.

These studies demonstrated the importance of cloud-radiation interactions for climate modeling, but they did not distinguish between cumulus cloudiness and supersaturation cloudiness. This distinction is important, first because of the difference in the fractional cloudiness associated with these two cloud types, second because of the different geographical and seasonal distributions of cumulus and stratus clouds, and finally because of the different vertical extents of these two cloud forms.

In the GLAS climate model, simulated clouds of any kind are assumed to fill an entire grid area, which is typically about 500 km x 400 km in the horizontal and 1 - 2 km in the vertical. The simulated cloud cover is used to determine the radiative heating and cooling of the atmosphere-earth system. In nature, the fractional cloudiness produced by cumulus convection is observed to be small (Malkus, 1958; Krishnamurti, 1968). This suggests the need for a parameterization of subgrid-scale convective cloudiness for use in the radiation parameterizations of the climate model.

The theory of subgrid-scale fractional cloudiness is still in an early stage of development. The interaction of finite clouds with solar radiation has been studied by McKee and Cox (1974, 1976), Davies (1978), and Davis et al. (1979a,b), and the interaction of finite clouds with infrared radiation has been discussed by Liou and Ou (1979), and Harshvardhan and Weinman (1982). A theory to determine the subgrid-scale cloudiness associated with shallow cumuli was proposed by Albrecht et al. (1979) and Albrecht (1979, 1981), while subgrid scale stratiform cloudiness has been parameterized by Sundqvist (1978, 1981). These studies represent progress towards the parameterization of cloudiness on unresolved scales, but the problem is so vast that much additional work is needed before a general parameterization suitable for global climate models can be created. In particular, there currently exists no theory to determine the fractional cloudiness associated with deep cumuli and their associated anvils and cirrus blowoff. Much of the cloudiness in the ITCZ and over the tropical and summer-hemisphere continents is believed to be associated with such convective complexes (e.g., Houze, 1977; Ogura and Chen, 1977).

Lacking a physically based parameterization to determine the subgrid-scale fractional cloudiness associated with cumulus convection, it may be better to neglect the cumulus cloudiness altogether than to treat it as overcast. The purpose of the present study is to examine the impact on the simulated general circulation as the cumulus cloud cover is changed from 100% (the control) to zero (the experiment) for purposes of calculating the solar and terrestrial radiative transfer. As will be shown, this change leads to some improvement in the simulated radiation budget of the earth. It also reveals the strength and nature of the sensitivity of the model to fractional cumulus cloudiness. It thus provides guidance and motivation for future efforts to incorporate into the model a realistic parameterization of subgrid-scale cumulus cloudiness.

2. Model description and initial conditions

The GLAS climate model has evolved from the GISS GCM, described by Somerville et al. (1974) and Stone et al. (1977), which in turn, was based on the 3-level 1970 version of the GCM developed by A. Arakawa and Y. Mintz at UCLA. The model uses a form of the σ coordinate system (Phillips, 1957), with nine layers, all of the same σ thickness, and a 4 x 5 degree latitude-longitude grid, which is modified in the polar regions as discussed below. The variables are staggered in the horizontal according to the B-grid scheme of Arakawa and Lamb (1977), and in the vertical according to the scheme of Lorenz (1960). The upper boundary of the model is at 10 mb. The prognostic atmospheric variables are the surface pressure, the zonal and meridional components of the horizontal wind, the temperature, and the water vapor mixing ratio. The prognostic boundary variables are the bulk ground temperature and ground wetness, and the snow depth.

Although the current model is similar to the GISS GCM presented by Somerville et al. (1974) and Stone et al. (1977), significant changes have been made in both the finite-difference schemes and the physical parameterizations. As described by Halem et al. (1979) and Herman and Johnson (1978), the model incorporates a "split grid," in which the number of grid points on a latitude circle is systematically reduced near the poles. This allows the use of a ten-minute time step, with only weak longitudinal smoothing at high latitudes. The idea is similar in principle to that proposed by Kurihara (1965), but is applied at only a few interfaces separating latitudinal bands within which the horizontal resolution is uniform. The resolution in each latitudinal band is twice that of its poleward adjacent neighbor. The differencing scheme for horizontal advection maintains the quasi-conservative properties of kinetic energy and mean-square vorticity, as in the Arakawa scheme. Although written to handle an arbitrary number of bands, the geometry used in the present model has five

latitudinal bands, consisting of a central region extending from -66° to +66°, bounded by one set of bands from 70° to 78°, and a second set from 82° to 86°. The latitudinal resolution is 4° in all bands. The longitudinal resolutions are 5°, 10°, and 20°, respectively.

Once every simulated half hour, a sixteenth-order Shapiro filter (Shapiro, 1970) is applied, in the longitudinal direction, to the sea level pressure, and to the potential temperature and the wind components on the σ surfaces. The filter was introduced as an ad hoc device to suppress the "checkerboard" noise in the prognostic fields, which arises from the inability of the B-grid to simulate the geostrophic adjustment process at the two grid interval level (Arakawa and Lamb, 1977).

The planetary boundary layer (PBL) parameterization was formulated by Katayama and modified by Somerville, et al. (1974) and Sud and Abeles (1981).

The model incorporates a prognostic soil moisture, with parameterizations of runoff, snow melt, and potential evapotranspiration, as developed by Lin et al. (1978).

The Matsuno forward-backward time differencing scheme is used. This scheme tends to damp high frequencies, and so it helps to control computational noise in the model, but at the cost of almost doubling the computing time required for the dynamics.

We use the cumulus parameterization developed by Arakawa (1969) for the three-level UCLA GCM; but as modified for use in a nine-level GCM by Somerville et al. (1974; see also Helfand, 1979). Although this Arakawa cumulus parameterization predates the Arakawa-Schubert cumulus parameterization (Arakawa and Schubert, 1974; Lord and Arakawa,1981; Lord, 1982; Lord, Chao, and Arakawa, 1982), many key concepts employed by Arakawa and Schubert were already present in the 1969 paper, including the cumulus mass flux, a spectrum of clouds, and

closure formulated in terms of the stabilization of the environment by the clouds. Helfand (1979) modified the parameterization to include very deep clouds and cumulus friction, but these modifications are not incorporated into the present model.

The model also includes latent heat release due to large-scale saturation, which occurs when the relative humidity exceeds 100%.

The short-wave radiation parameterization is that presented by Lacis and Hansen (1974). It includes absorption by ozone, water vapor, and clouds.

The long-wave radiation parameterization of the current model is based on the method of Wu (1976), Wu et al. (1978), and Wu (1980), as described by Krishnamurthy (1982). The parameterization includes a water vapor transmittance that uses a statistical band model with the strong line version of the Curtis-Godson (Godson, 1955) approximation; the water vapor dimer effect in the 8-13 μ window region; line-by-line precalculation of CO_2 transmittance including fundamental bands, hot bands, and isotopes; tables of ozone transmittance calculated by Dr. N. Scott (private communication); a special treatment of the nearby layer quadrature for increased accuracy in the numerical integration; and the effects of clouds. In order to calculate the incoming long wave flux at the 10 mb level, the top of the model, zonally averaged climatological temperatures at 1 mb and 5 mb are prescribed. In order to save computing time, the time step for the long-wave radiation is five hours for the simulations presented in this paper.

Clouds are assumed to occur if and only if the model predicts cumulus convection (restricted to the lowest six layers) or large-scale saturation (in any layer). In keeping with the earlier discussion, no parameterization of subgrid-scale fractional cloudiness is attempted. In the control run described in this paper, both supersaturation and convective clouds are assumed to completely

fill a grid box. In the experiment, supersaturation clouds are again assumed to completely fill a grid box, but convective clouds are ignored. For the solar radiation parameterization, the optical properties of the clouds are prescribed as shown in Table 1. For the terrestrial radiation parameterization, all clouds are assumed to be black bodies.

In both runs, the model was initialized with the observed conditions for 15 June, 1979, and integrated for 45 days. The July mean results are obtained by averaging the output data through the last 31 days. Although history records were written only every 12 simulated hours, the radiation, cloudiness, and precipitation results presented in the next section ware accumulated between writes to the tape, so that there are no sampling errors in these results.

3. Results

The most significant differences between the two simulations are in the radiation budget, as expected, and in the temperature field. The feedback between cumulus convection and radiation also appears to be significant. We first show the cloud fields and the radiation budget; the effects on the other fields then become clear.

3.1 Cloudiness. The cloud field has been analyzed to determine the global distribution and the zonal average of the July-mean frequency of cloudiness. The monthly mean cloud frequency is defined as the fraction of the time for which cloud occurs within the month. It has been obtained separately for cumulus clouds and supersaturation clouds.

Figs. 1a and 1b show the geographical distribution of the cumulus cloud frequency in layer 6 (about 500 mb), for control and experiment, respectively. Cumulus clouds occur somewhat less frequently over land in the experiment than in the control. This is true mainly for the deep clouds. The zonal-mean cumulus cloud frequency (Fig. 2) is reduced in the experiment everywhere over land by a few percent, except near 30°N and 30°S. Detailed examination of the model results shows that if we consider only deep cumulus clouds, the zonal-mean cloud frequency is reduced in the experiment not only over land, but also over ocean.

When the model treats cumulus clouds as having 100% fractional cloud cover, there typically is strong long-wave cooling near the cloud top, and solar heating lower in the cloud. Radiative heating and cooling thus tend to steepen the lapse rate in the cloud layer, favoring stronger moist convection. This is why neglecting the radiative effects of cumulus cloudiness leads to reduced cumulus activity in the model.

Helfand (1981) noted that the GLAS model produces very intense cumulus convection over land in summer. He showed that the simulated level of convective activity can be reduced by requiring that the relative humidity at the cloud base level exceed 95% as a precondition for convection. Our results show that the simulated convective activity over land in summer can also be reduced by neglecting the radiative effects of the cumulus clouds. Undoubtedly there are still more ways to reduce the simulated level of convective activity.

For both the experiment and the control, the supersaturation cloud frequency over the oceans is excessive in comparison with observations. Fig. 3 shows that much of the excessive supersaturation cloudiness occurs in the lowest model layer. The zonal-mean supersaturation cloudiness (Fig. 4) is increased in the experiment over the ocean (but not over land). The increased supersaturation cloudiness tends to make up for the elimination of the cumulus cloudiness over the ocean. At the land points, there is a net reduction in cloudiness.

3.2 Radiation. At the top of the atmosphere, the zonal-mean net radiation flux into the atmosphere (Fig. 5) is larger in the experiment, by about 20 W m^{-2}, between 10-60°N. In the experiment, the local minimum of the radiation flux at about 26°N is due to increased oceanic supersaturation cloudiness. The results of the control run are in better agreement with observations obtained from satellite data of June 1974-February 1978 (Winston, et al., 1979). However, a separate examination of the solar and thermal radiation streams indicates three characteristics of the radiation balance (Figs. 6 and 7). First, for each component of the radiation flux, the experiment shows better results than the control. The control underestimates both the outgoing thermal radiation and the incoming solar radiation more severely than the experiment, but these errors tend to cancel; as a result, the control produces a better simulation of the net radiation balance of the earth-atmosphere system. Second, the larger

net incoming radiation flux in the summer hemisphere in the experiment, relative to that in the control, is chiefly due to a reduction in the albedo; the cloud albedo effect dominates the cloud greenhouse effect. Third, both runs systematically underestimate the net outgoing thermal radiation by about 40 W m^{-2} at all latitudes. We will come back to this point later.

At the earth's surface, the zonal-mean net radiation flux (Fig. 8) in the experiment is larger than that in the control, especially near the ITCZ (approximately 10°N) and in the mid-latitude cyclone zone (30-60°N). This is mainly due to reduced screening of solar radiation in the experiment. The difference reaches 15 W m^{-2}, which is about 8% of the total flux. This difference occurs mainly over land, where the model produces more cumulus clouds. In the experiment, the zonally averaged surface radiation flux over land increases, relative to the control run, by about 20% of the total flux. For reference, the observed surface net radiation flux is also shown (Schutz and Gates, 1972), although it is important to keep in mind the uncertainties of the observations. The experiment produces more solar radiation into the earth's surface than the control in the summer hemisphere (Fig. 9), except near 26°N where the experiment has increased supersaturation cloudiness. Fig. 10 shows that the two simulations have about the same surface thermal radiation flux.

Fig. 11 shows that the net surface radiation flux has increased in the experiment by about 20-60 W m^{-2} over Asia, North America, and central Africa. These locations of large differences coincide well with those of maximum frequency of cumulus clouds (Fig. 1).

Herman (1980) suggested two possible explanations for the apparent failure of the GLAS model to emit enough thermal radiation to space. First, he noted that in the model cumulus clouds are unrealistically assumed to cover the entire grid area. In our experiment, we have completely removed the radiative effects

of cumulus clouds, and in most latitudinal belts, the resulting increase in the outgoing thermal radiation is about 10 W m^{-2} (Fig. 7). A further increase of 30 W m^{-2} is needed.

Second, Herman pointed out that the model does not properly take into account the semi-transparent properties of thin, high cirrus clouds; these clouds are unrealistically assumed to be black bodies, opaque to the terrestrial radiation upwelling from the earth's surface. In a separate experiment, Shukla (personal communication, 1981) made all clouds in the top three layers of the model (above about 300 mb) transparent to both solar and terrestrial radiation, without changing the radiative effects of the cumulus clouds, which in any case do not penetrate the top three layers. In Shukla's experiment, the net upward longwave radiation at the top of the atmosphere increased by about 30 W m^{-2} on an average between 30°S and 30°N, and increased by about 5 W m^{-2} on the average at middle latitudes. The tropical fluxes were thus brought into reasonable agreement with observations, but the middle-latitude fluxes remained much too small. In contrast, the results of the present experiment (Fig. 7) show relatively little change in the tropics, but a noticeable improvement at middle latitudes.

We have found that part of the deficiency in the outgoing thermal flux to space is due to the model's overprediction of low-level supersaturation clouds. In both simulations, the July cloud frequency for supersaturation clouds in the lowest model layer over the ocean is twice that observed (see again Fig. 4). The simulated low stratiform cloudiness is about 20% more than observed, south of 30°N. These low-level clouds strongly emit thermal radiation downward to the earth's surface. For black-body emission, and assuming a 10°C temperature difference between the surface and the top of the low clouds, the excessive low-level clouds lead us to underestimate the simulated outgoing thermal radiation by about 12 W m^{-2}.

3.3 Temperature and winds. Because of the larger radiation input into the earth's surface, the ground temperatures over Asia, North America, and Africa are 3-6°C warmer in the experiment (Fig. 12). This is in agreement with the results of Meleshko and Wetherald's (1981) study of the effect of a prescribed geographical distribution of clouds on climate. In their experiment, a reduction in continental cloudiness results in warmer continents. As in their study, lower sea level pressures (Fig. 13) are obtained in our experiment over Asia, North America, and Africa. Over Australia, very few cumulus clouds occur; the warming in northern Australia is due to a change of the large-scale low-level wind direction from southeasterly in the control to easterly in the experiment, which can be seen from the sea level pressure field.

In the experiment, the atmosphere is generally warmer in the Northern (summer) Hemisphere (Fig. 14). This warming is due to the larger net radiation input at the top of the atmosphere (see again Fig. 5), which results from the fact that less solar radiation is reflected back to space in the experiment. The largest increase occurs in the upper troposphere[1], near the tops of the deep cumulus clouds. Detailed examination of the output from the control simulation shows that the magnitude of the long-wave cooling near the top of the clouds is typically larger than the solar heating inside the clouds. Therefore, long-wave cooling dominates the solar heating, especially in the upper troposphere. The experiment includes no radiative heating or cooling inside the cumulus clouds, and hence has warmer air in the upper troposphere.

The higher temperature in the Northern Hemisphere in the experiment reduces the zonal-mean meridional temperature gradient, and therefore decreases the vertical shear of the zonal-mean zonal wind in the subtropics. Consequently,

---

[1] At the poles, there is only one grid point. Therefore, large differences between two simulations at the poles are not meaningful.

the zonal-mean zonal wind in the experiment is easterly throughout the whole subtropical troposphere (Fig. 15).

3.4 Precipitation. Both simulations give about the same zonal-mean total precipitation (Fig. 16), except in the tropics and in the summer monsoon region near 26°N. The experiment produces increased convective precipitation in the coastal regions of the warm continents, near 26°N, as a result of the intensification of monsoonal circulations associated with the warmer land in the experiment. Meleshko and Wetherald (1981) reported a similar finding. This suggests that monsoonal cloudiness may serve as a regulator of the monsoon circulations. A weak monsoon may produce relatively little cloudiness, allowing the continent to warm up, and thereby leading to an intensification of the monsoon. The extensive cloudiness associated with a strong monsoon may reduce the land-sea thermal contrast, thus tending to weaken the monsoon circulation.

Fig. 17 shows the zonal-mean precipitation due to convective clouds only; here the control has a well-defined ITCZ but the experiment does not. By analyzing the convective precipitation over land and ocean, separately, we find that the control produces the tropical convection maximum at 10°N over both land and ocean, while the experiment produces the maximum over land at 10°N and a maximum over the ocean near the equator. As a result, the experiment does not show a well-defined tropical peak of the zonal-mean convective precipitation.

4. Summary

In the real atmosphere, convective clouds typically have much smaller horizontal extent, and hence much less effect on the radiation balance, than supersaturation clouds. For both types of clouds, the GLAS climate model assigns 100% fractional cloud cover for a grid area to compute the radiation field. There is currently no method to parameterize the fractional cloudiness associated with deep convection. It may be better to assume zero cloudiness for convective clouds and 100% for supersaturation clouds. In this paper, we report a comparison between an experiment in which cumulus clouds are assumed to be radiatively inactive, and a control in which cumulus clouds are assumed to produce 100% fractional cloud cover.

The control produces a closer agreement with the satellite-observed net radiation flux at the top of the atmosphere than the experiment. By separately analyzing the solar and thermal radiation fluxes at the top of the atmosphere, we find that the control underestimates both observed solar input and thermal output more than the experiment does, but by a cancellation of the larger errors, produces a better net radiation budget of the earth-atmosphere system.

Over the whole globe, the zonal-mean thermal radiation flux from the earth's surface to the atmosphere and from the atmosphere to space are both systematically underpredicted by about 40 W m^{-2} in both simulations, though the deficit is smaller in the experiment. These discrepancies partly result from an overestimation of low-level supersaturation clouds in the model. To significantly improve the model's simulation of cloudiness, it is therefore necessary not only to improve the parameterization of convective fractional cloudiness, but also to improve the parameterization of the turbulent transfer processes in the planetary boundary layer. An improved planetary boundary layer parameterization may prevent the overproduction of supersaturation clouds in the lowest layer.

The comparison between two simulations shows a significant impact of the cumulus cloud-radiation interaction on model climatology. The cloud albedo effect dominates the greenhouse effect, and so neglecting the cumulus cloudiness produces more net radiation input into the earth-atmosphere system. As a consequence, the zonal-mean temperature is higher in the experiment. The warmer air occurs mainly over land, since the sea surface temperature is fixed in the model. It is clear that the climatic effect of the cumulus cloud-radiation interaction will be even larger in a coupled ocean-atmosphere climate model. In this light, efforts to parameterize subgrid-scale cumulus (and stratus) cloudiness are seen to be of great importance.

Acknowledgements

We thank several of our colleagues for helpful reviews, particularly, Professors Yale Mintz and Gerald Herman. We also thank Debbie Boyer for patiently typing numerous revisions.

References

Albrecht, B. A., A. K. Betts, W. H. Schubert, and S. K. Cox, 1979: A model of the thermodynamic structure of the trade-wind boundary layer: Part I. Theoretical formulation and sensitivity tests. J. Atmos. Sci., 36, 73-89.

Albrecht, B. A., 1979: A model of the thermodynamic structure of the trade-wind boundary layer: Part II. Applications. J. Atmos. Sci., 36, 90-98.

Albrecht, B. A., 1981: Parameterization of trade-cumulus cloud amounts. J. Atmos. Sci., 38, 97-105.

Arakawa, A., 1969: Parameterization of cumulus convection. Proc. WMO/IUGG Symposium on Numerical Prediction in Tokyo, IV8, 1-6.

Arakawa, A., and W. H. Schubert, 1974: The interaction of a cumulus cloud ensemble with the large-scale environment, Part I. J. Atmos. Sci., 31, 674-701.

Arakawa, A., and V. R. Lamb, 1977: Computational design of the basic dynamical processes of the UCLA general circulation model. Methods in Computational Physics, 17, Academic Press, New York, 173-265.

Davies, R., 1978: The effect of finite geometry on the three-dimensional transfer of solar irradiance in clouds. J. Atmos. Sci., 35, 1712-1725.

Davis, J. M., S. K. Cox, and T. B. McKee, 1979a: Total shortwave radiative characteristics of absorbing finite clouds. J. Atmos. Sci., 36, 508-518.

Davis, J. M., S. K. Cox, and T. B. McKee, 1979b: Vertical and horizontal distribution of solar absorption in finite clouds. J. Atmos. Sci., 36, 1976-1984.

Godson, W. L., 1955: The computation of infrared transmission by atmospheric water vapor. J. Meteorol., 12, 272-284.

Halem, M., J. Shukla, Y. Mintz, M. L. Wu, R. Godbole, G. Herman, and Y. Sud, 1979: Comparison of observed seasonal climate features with a winter and summer numerical simulation produced with the GLAS general circulation model. GARP Publication Series No. 22, 207-253, World Meteorological Organization, Case postale No. 5, CH-1211 Geneva 20, Switzerland.

Harshvardhan, and J. A. Weinman, 1982: Infrared radiative transfer through a regular array of cuboidal clouds. J. Atmos. Sci., 39, 431-439.

Helfand, H. M., 1979: The effect of cumulus friction on the simulation of the January Hadley circulation by the GLAS model of the general circulation. J. Atmos. Sci., 36, 1827-1843.

Helfand, H. M., 1981: Dependence of tropospheric temperature on the parameterization of cumulus convection in the GLAS model of the general circulation. Mon. Wea. Rev., 109, 65-76.

Herman, G. F., and W. T. Johnson, 1978: The sensitivity of the general circulation to Arctic sea ice boundaries: A numerical experiment. Mon. Wea. Rev., 106, 1649-1664.

Herman, G. F., M.-L. C. Wu, and W. T. Johnson, 1980: The effect of clouds on the earth's solar and infrared radiation budgets. J. Atmos. Sci., 37, 251-1261.

Herman, G. F., 1980: Cloud-radiation experiments conducted with GLAS general circulation models. Workshop on Radiation and Cloud-Radiation Interaction in Numerical Modeling at the European Centre for Medium-Range Weather Forecasts, Reading, England, 15-17 October, 1980, p. 75-112.

Houze, R. A., 1977: Structure and dynamics of a tropical squall-line system. Mon. Wea. Rev., 105, 1540-1567.

Jaeger, L., 1976: Monatskarten des Niederschlags fue die ganze Erde. Berichte des Deutschen Welterdienstes, 18, No. 139. Im Selbstverlag des Deutchen Welterdienstes, Offenbach, W. Germany.

Krishnamurthy, V., 1982: The documentation of the Wu-Kaplan radiation parameterization. NASA Tech. Memo. 83926, 93 pp.

Krishnamurti, T. N., 1968: A calculation of percentage area covered by convective clouds from moisture convergence. J. Appl. Meteor., 7, 184-195.

Kurihara, Y., 1965: Numerical integration of the primitive equations on a spherical grid. Mon. Wea. Rev., 93, 399-415.

Lacis, A. A., and J. E. Hansen, 1974: A parameterization for the absorption of solar radiation in the earth's atmosphere. J. Atmos. Sci., 31, 118-133.

Lin, J. D., J. Alfano, and P. Bock, 1978: Documentation of a ground hydrology parameterization for use in the GISS general circulation model. NASA CR158766, 143 pp.

Liou, K.-N., and S.-C. Ou, 1979: Infrared radiative transfer in finite cloud layers. J. Atmos. Sci., 36, 1985-1996.

Lord, S. J., and A. Arakawa, 1980: Interaction of a cumulus ensemble with the large-scale environment. Part II. J. Atmos. Sci., 37, 2677-2692.

Lord, S. J., 1982: Interaction of a cumulus cloud ensemble with the large-scale environment. Part III. Semi-prognostic test of the Arakawa-Schubert cumulus parameterization. J. Atmos. Sci., 39, 88-103.

Lord, S. J., W. C. Chao, and A. Arakawa, 1982: Interaction of a cumulus cloud ensemble with the large-scale environment. Part IV. The discrete model. J. Atmos. Sci., 39, 104-113.

Lorenz, E. N., 1960: Energy and numerial weather prediction. Tellus, 12, 364-373.

Malkus, J. S., 1958: On the structure of the trade wind moist layer. Pap. Phys. Oceanogr. Meteor., 13, 1-47.

McKee, T. B., and S. K. Cox, 1974: Scattering of visible radiation by finite clouds. J. Atmos. Sci., 31, 1885-1892.

McKee, T. B., and S. K. Cox, 1976: Simulated radiance patterns for finite cubic clouds. J. Atmos. Sci., 33, 2014-2020.

Meleshko, V. P., and R. T. Wetherald, 1981: The effect of a geographical cloud distribution on climate: A numerical experiment with an atmospheric general circulation model. J. Geophys. Res., 86, 11995-12014.

Ogura, Y., and Y. Chen, 1977: A life history of an intense mesoscale convective storm in Oklahoma. J. Atmos. Sci., 34, 1458-1476.

Phillips, N. A., 1957: A coordinate system having some special advantages for numerical forecasting. J. Meteor., 14, 184-185.

Schutz, C., and W. L. Gates, 1972: Global Climatic Data for Surface, 800 mb, 400 mb: July. Advanced Research Projects Agency, Rand, Santa Monica, California. R-1029-ARPA. ARPA Order No. 189-1.

Shapiro, R., 1970: Smoothing, filtering, and boundary effects. Rev. Geophys. and Space Phys., 8, 359-387.

Shukla, J., and Y. Sud, 1981: Effect of cloud-radiation feedback on the climate of a general circulation model. J. Atmos. Sci., 38, 2337-2353.

Somerville, R. C., P. H. Stone, M. Halem, J. E. Hansen, J. S. Hogan, L. M. Druyan, G. Russel, A. A. Lacis, W. J. Quirk, and J. Tenenbaum, 1974: The GISS model of the global atmosphere. J. Atmos. Sci., 31, 84-117.

Stone, P. H., S. Chow, and W. J. Quirk, 1977: The July climate and a comparison of the January and July climates simulated by the GISS general circulation model. Mon. Wea. Rev., 105, 170-194.

Sud, Y. C., and J. A. Abeles, 1981: Calculation of surface temperature and surface fluxes in the GLAS GCM. NASA Tech. Memo. 82167.

Sundqvist, H., 1978: A parameterization scheme for non-convective condensation including prediction of cloud water content. Quart. J. Roy. Met. Soc., 104, 677-690.

Sundqvist, H., 1981: Prediction of stratiform clouds: Results from a 5-day forecast with a global model. Tellus, 33, 242-253.

Winston, J. S., A. Gruber, T. I. Gray, M. S. Varnadore, C. L. Earnest, and L. P. Mannello, 1979: Earth-atmosphere radiation budget analyses derived from NOAA satellite data, June 1974-February 1978, Vol. 2, U.S. Dept. of Commerce, NESS/NOAA, NTIS #PB80106867.

Wu, M. L., 1976: Longwave radiation and its effect on the atmosphere. Ph.D. Thesis, The University of Chicago, 160 pp.

Wu, M. L., L. D. Kaplan, and R. Godbole, 1978: Influence of systematic radiation differences on the dynamics of a model atmosphere. Third Conf. on Atmos. Rad. of the Amer. Meteor. Soc., June 28-30, 1978, Davis, California.

Wu, M. L., 1980: The exchange of infrared radiative energy in the troposphere. J. Geophys. Res., 85, 4084-4090.

Table 1. Prescribed cloud optical properties used in the GLAS solar radiation parameterization.

Cloud Form	Cloud Level	Cloud Type	Albedo (%)	Optical Thickness
Convective (control run only)	mid-level	Ac	50	8
	low-level	Cu	70	16
	penetrating	Cb	80	32
Super-Saturation	0-400 mb	Ci	20	2
	400-700 mb	As	50	8
	700-1000 mb	St	70	16

Figure Legends

Figure 1: Simulated July convective cloud frequency for model layer 6 (about 500 mb) for (a) the control and (b) the experiment. The contour interval is 20% and values greater than 40% are hatched.

Figure 2: Simulated July zonal-mean convective cloud frequency averaged (a) over ocean and (b) over land.

Figure 3: July zonal-mean supersaturation cloud frequency in the lowest model layer. The observations are from London (1957) and Van Loon et al. (1972), as shown in Meleshko and Wetherald (1981).

Figure 4: Simulated July zonal-mean supersaturation cloud frequency averaged (a) over ocean and (b) over land.

Figure 5: Zonally-averaged net total radiation flux from space into the atmosphere. The observed data are from Winston et al. (1979).

Figure 6: Same as Fig. 5, except for net solar radiation only.

Figure 7: Same as Fig. 5, except for net terrestrial radiation only (positive upward to space).

Figure 8: Zonally-averaged net total radiation flux into the earth's surface. The observed data are from Budyko (1963), as given by Schutz and Gates (1972).

Figure 9: Same as Fig. 8, except for net solar radiation only.

Figure 10: Same as Fig. 8, except for net terrestrial radiation only (positive upward from the earth's surface).

Figure 11: Global distribution of the difference (the experiment minus the control) in the net radiation flux into the earth's surface. The contour interval is 20 W m^{-2}. Values greater than 20 W m^{-2} are hatched.

Figure 12: Global distribution of the difference (the experiment minus the control) of the ground temperature. The contour interval is 2°C. Values greater than 2°C are hatched.

Figure 13: Sea level pressure (a) of the control and (b) of the experiment. The contour interval is 4 mb.

Figure 14: Difference (the experiment minus the control) of the zonal-mean temperature.

Figure 15: Latitude-height section of the zonal-mean of the zonal wind component (a) for the control, and (b) for the experiment.

Figure 16: Zonal-mean of the observed and simulated July mean total precipitation. The observations are from Jaegger (1976).

Figure 17: Zonal mean of the simulated July mean convective precipitation.

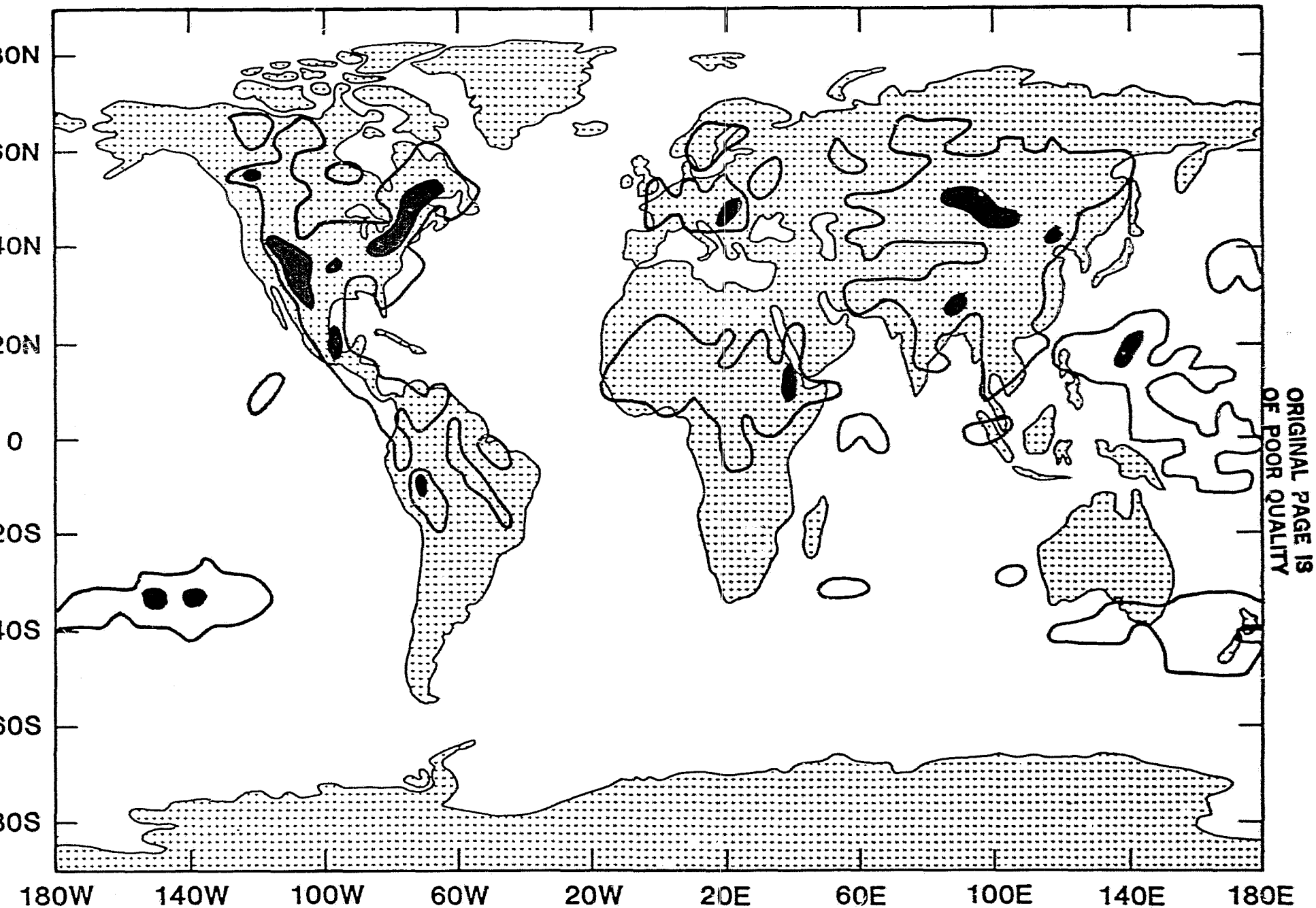

Figure 1a

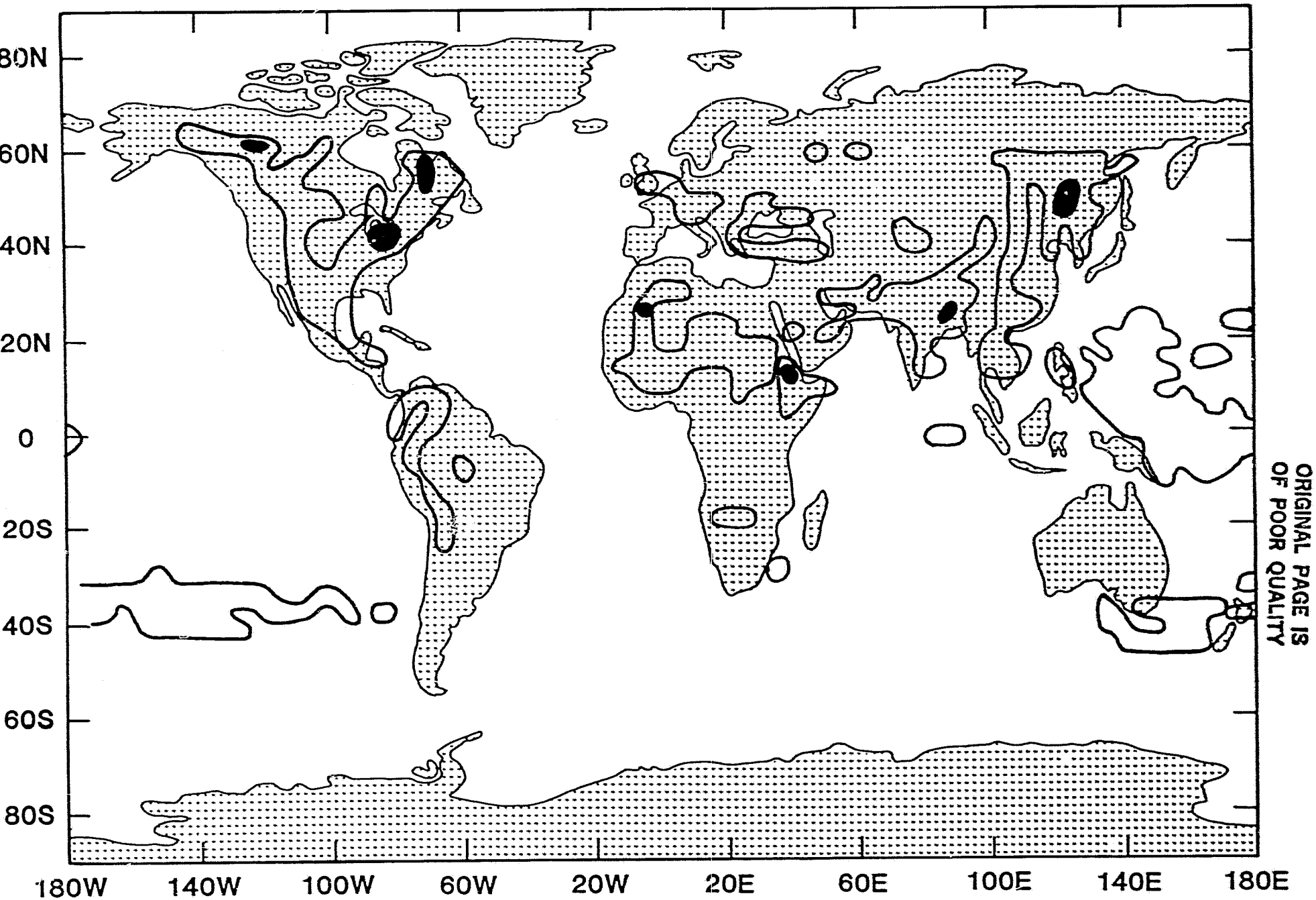

Figure 1b

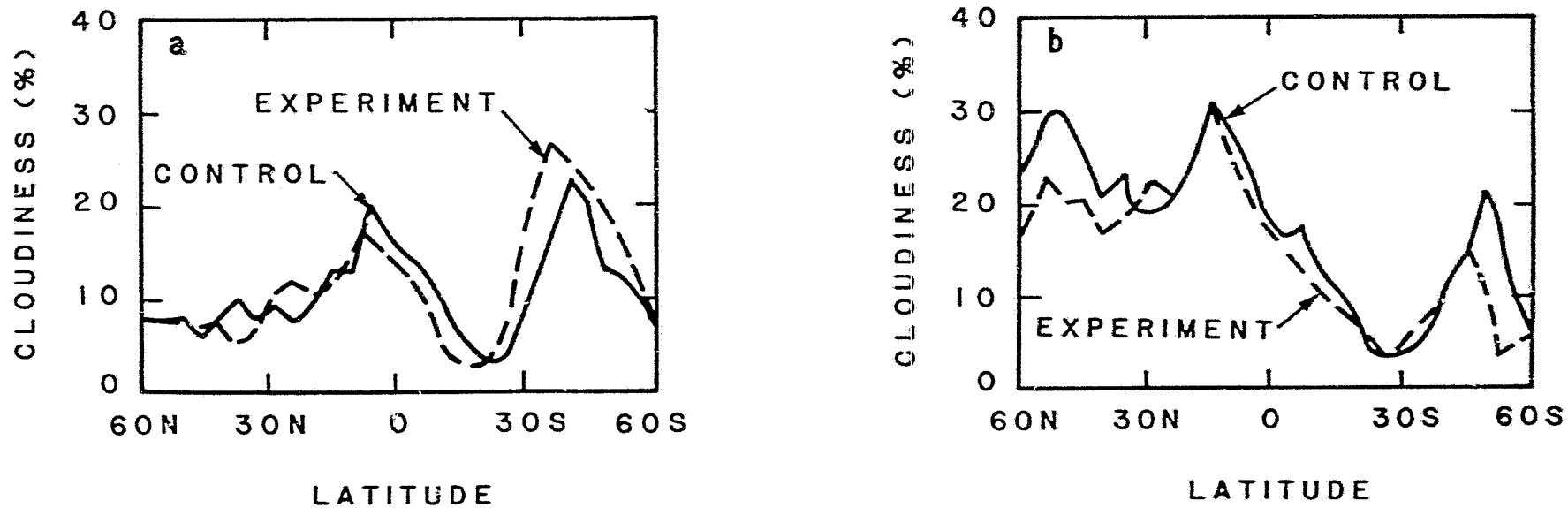

Figure 2

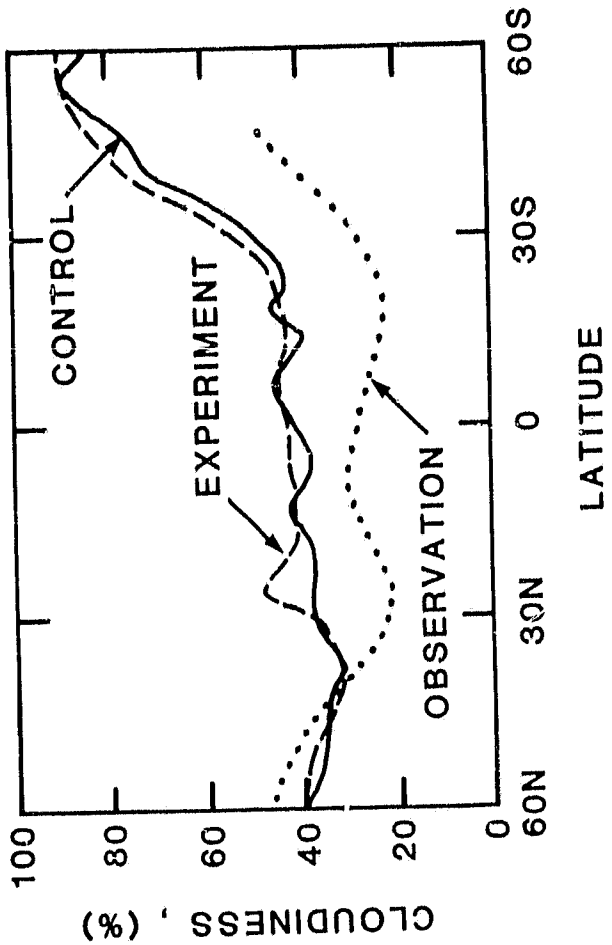

Figure 3

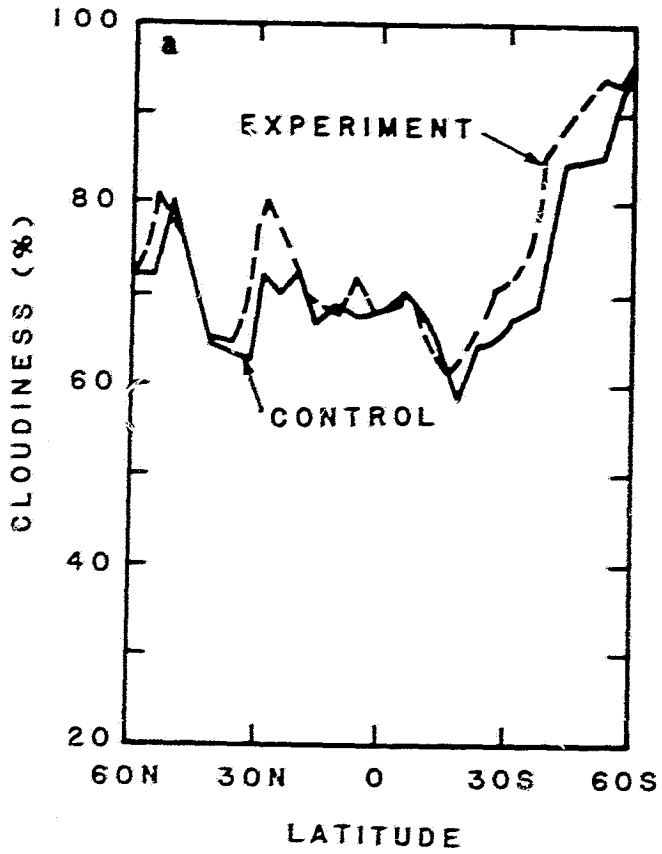

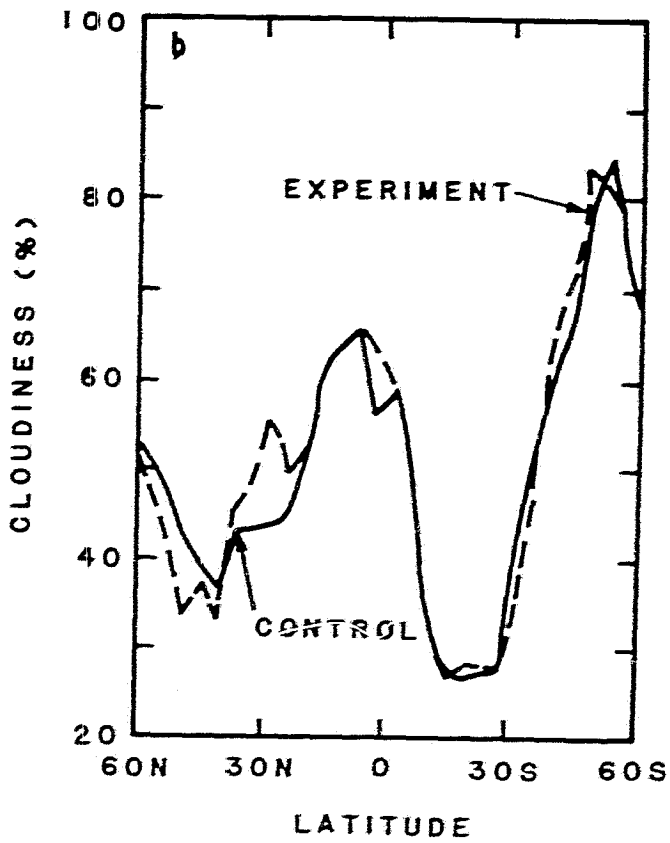

Figure 4

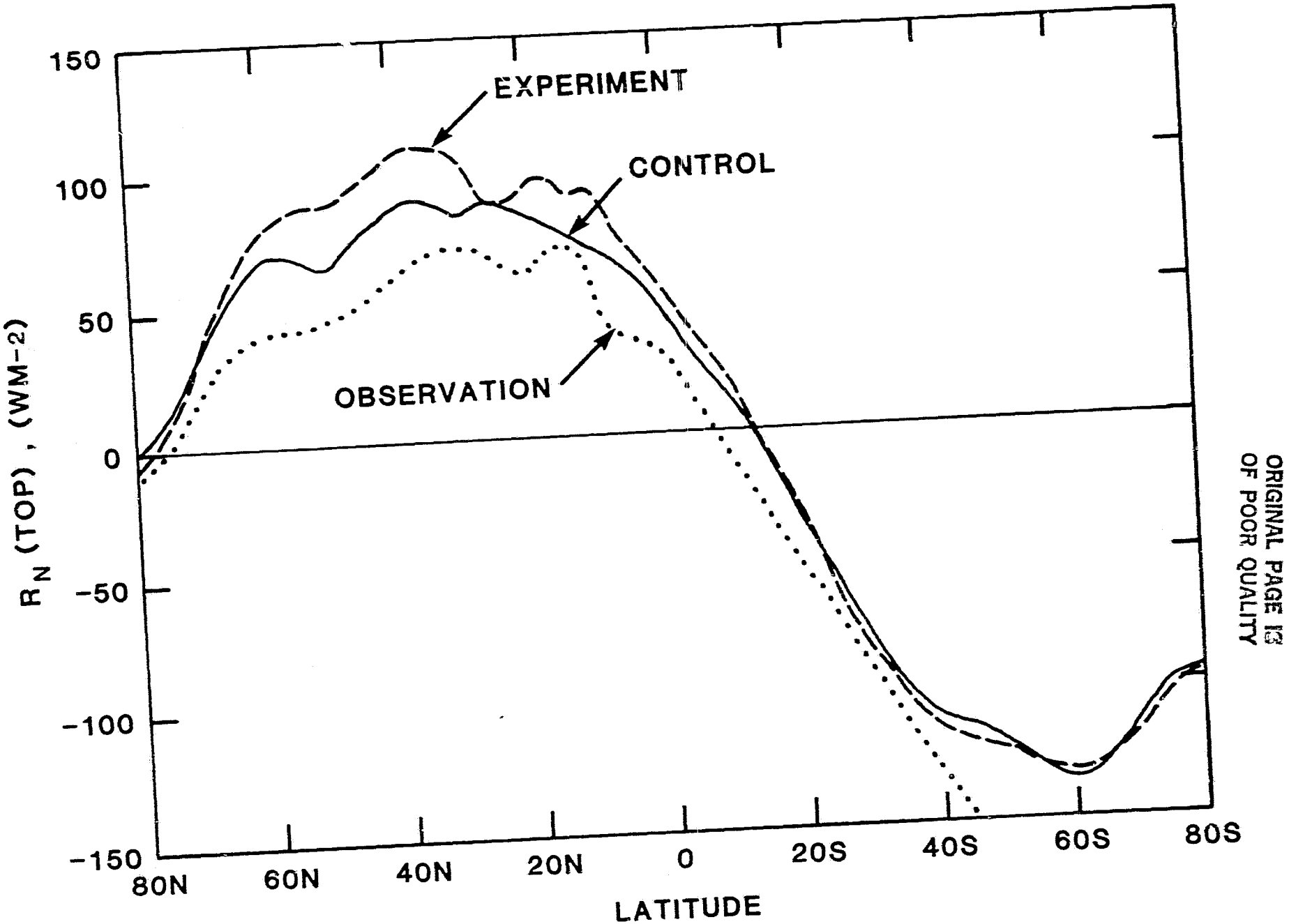

Figure 5

ORIGINAL PAGE IS
OF POOR QUALITY

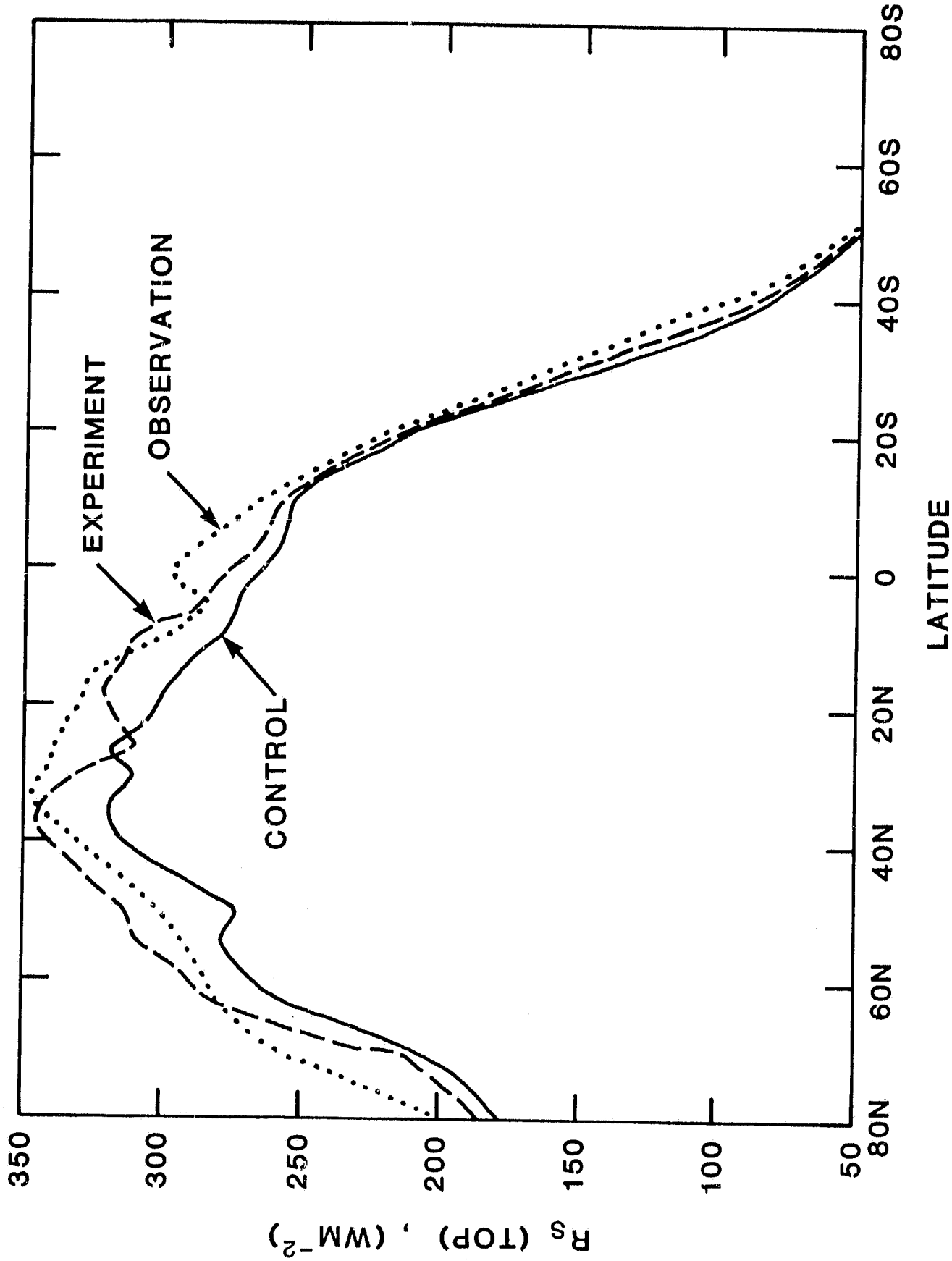

Figure 6

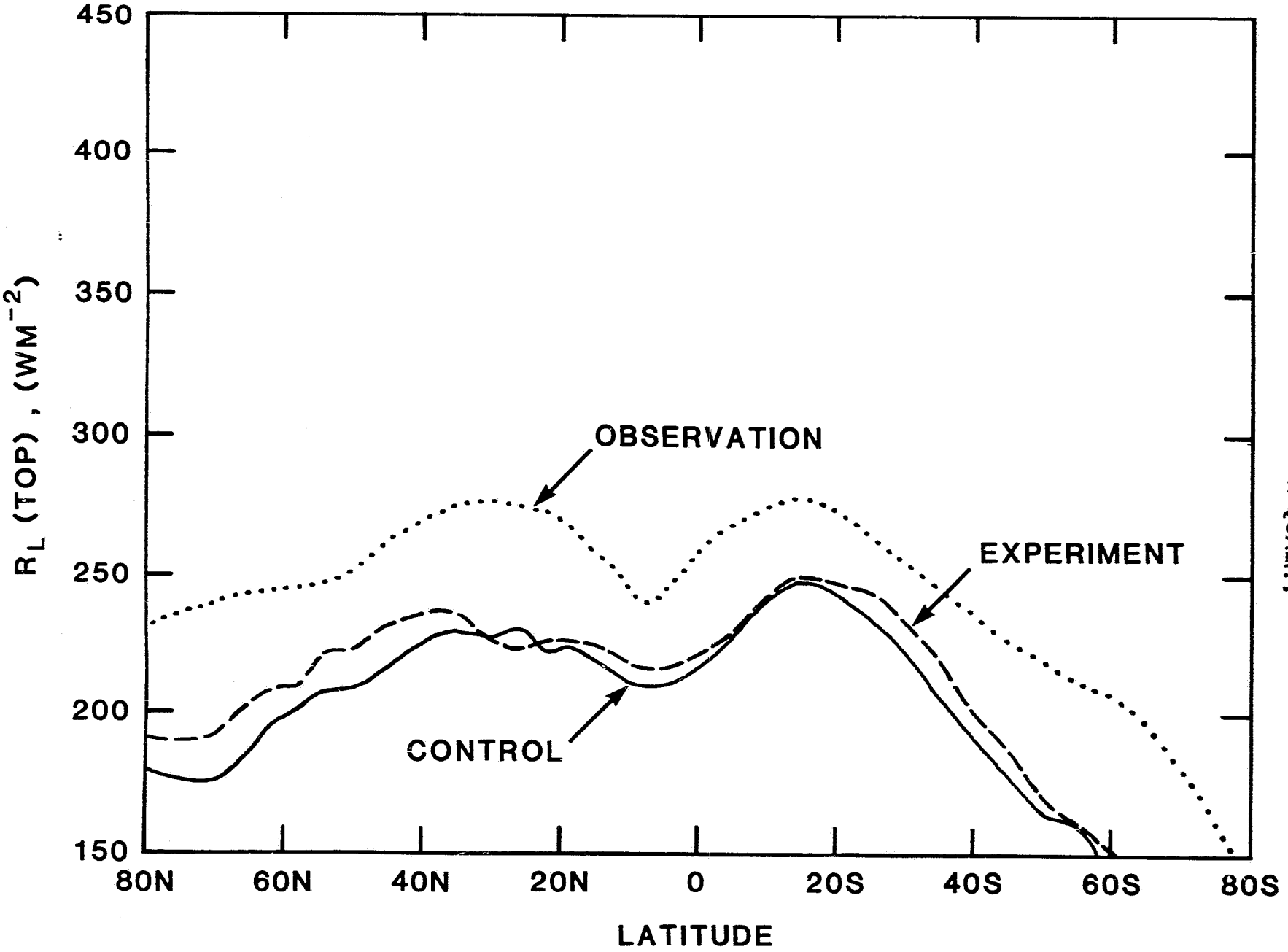

Figure 7

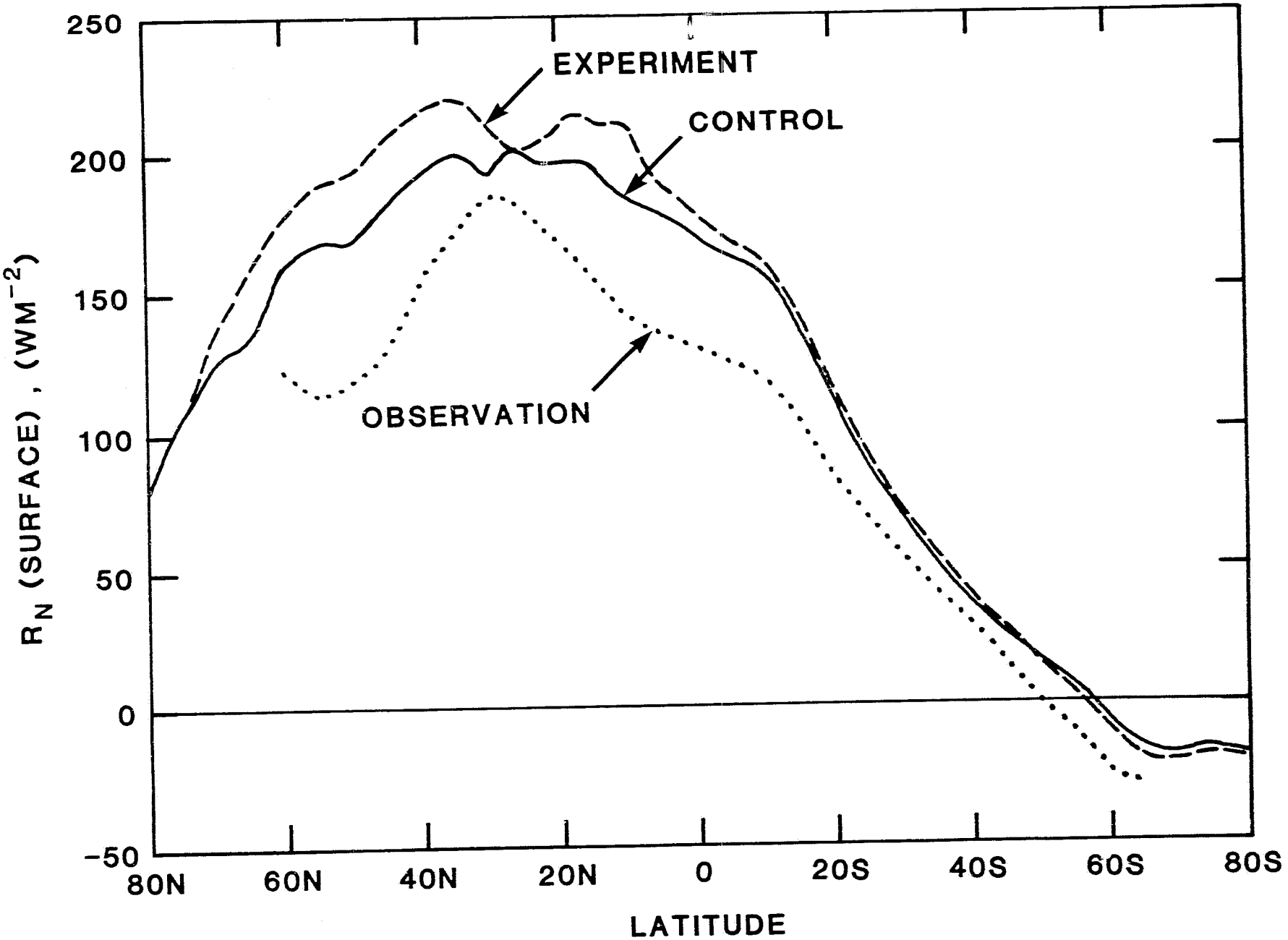

Figure 8

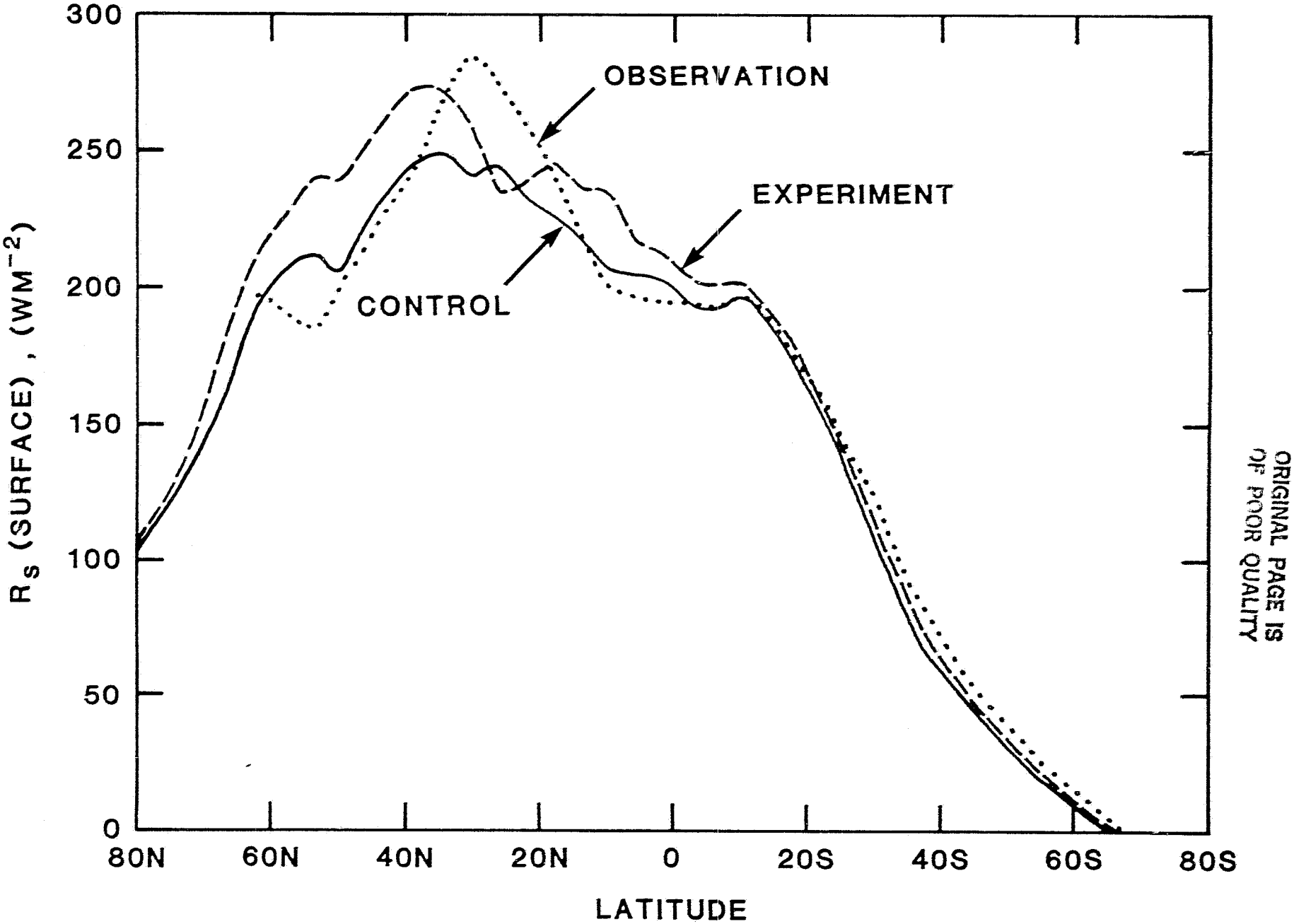

Figure 9

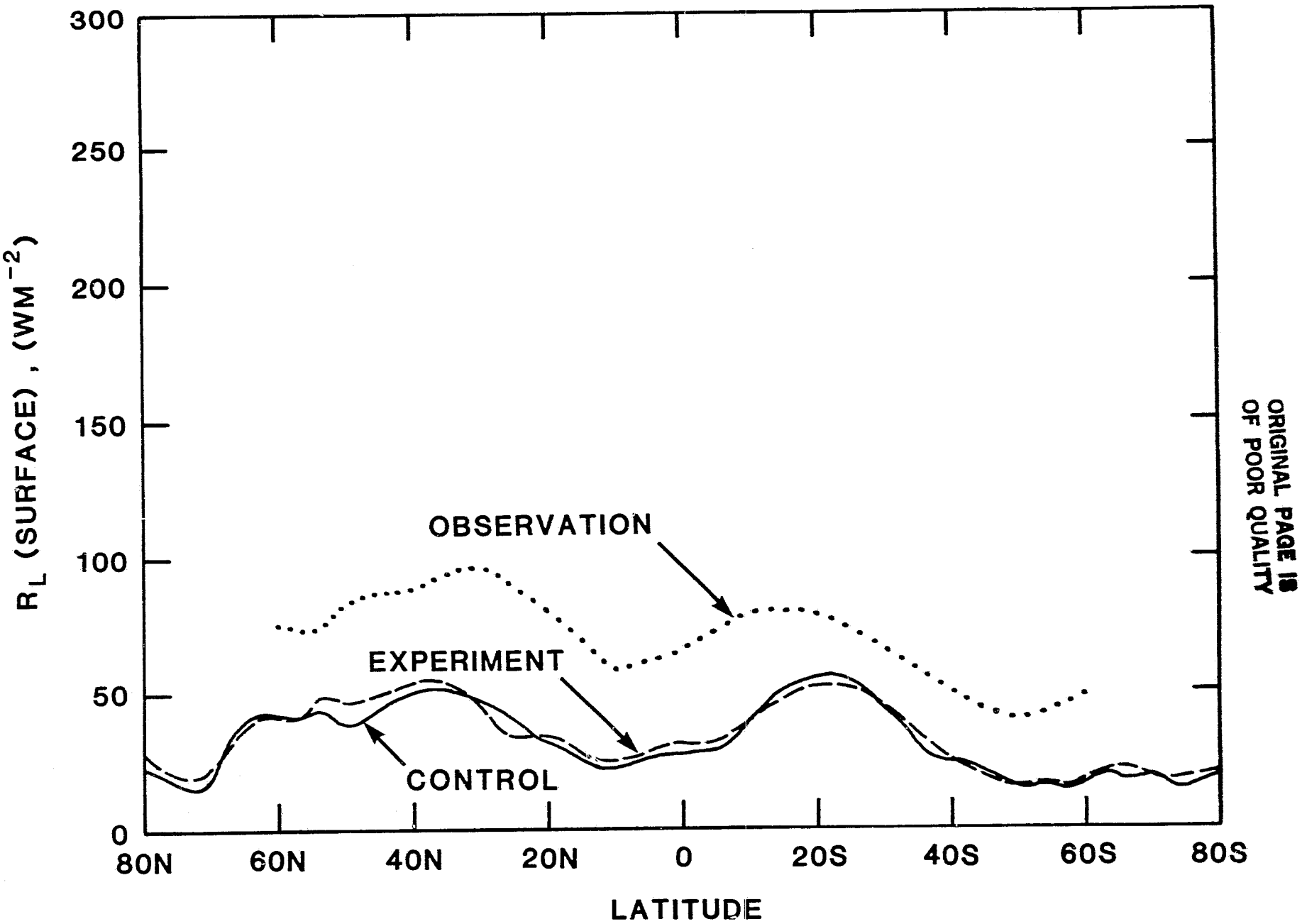

Figure 10

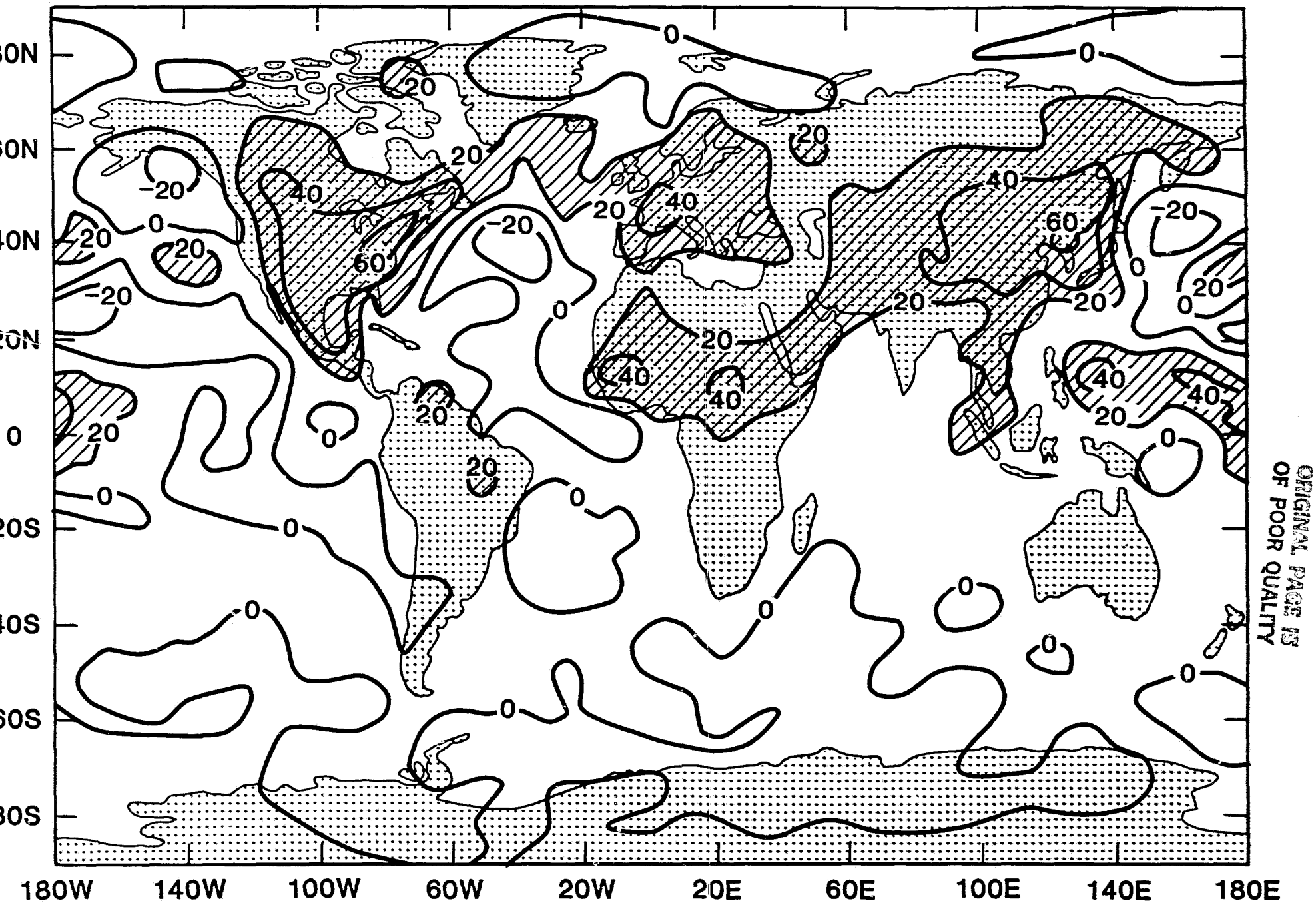

Figure 11

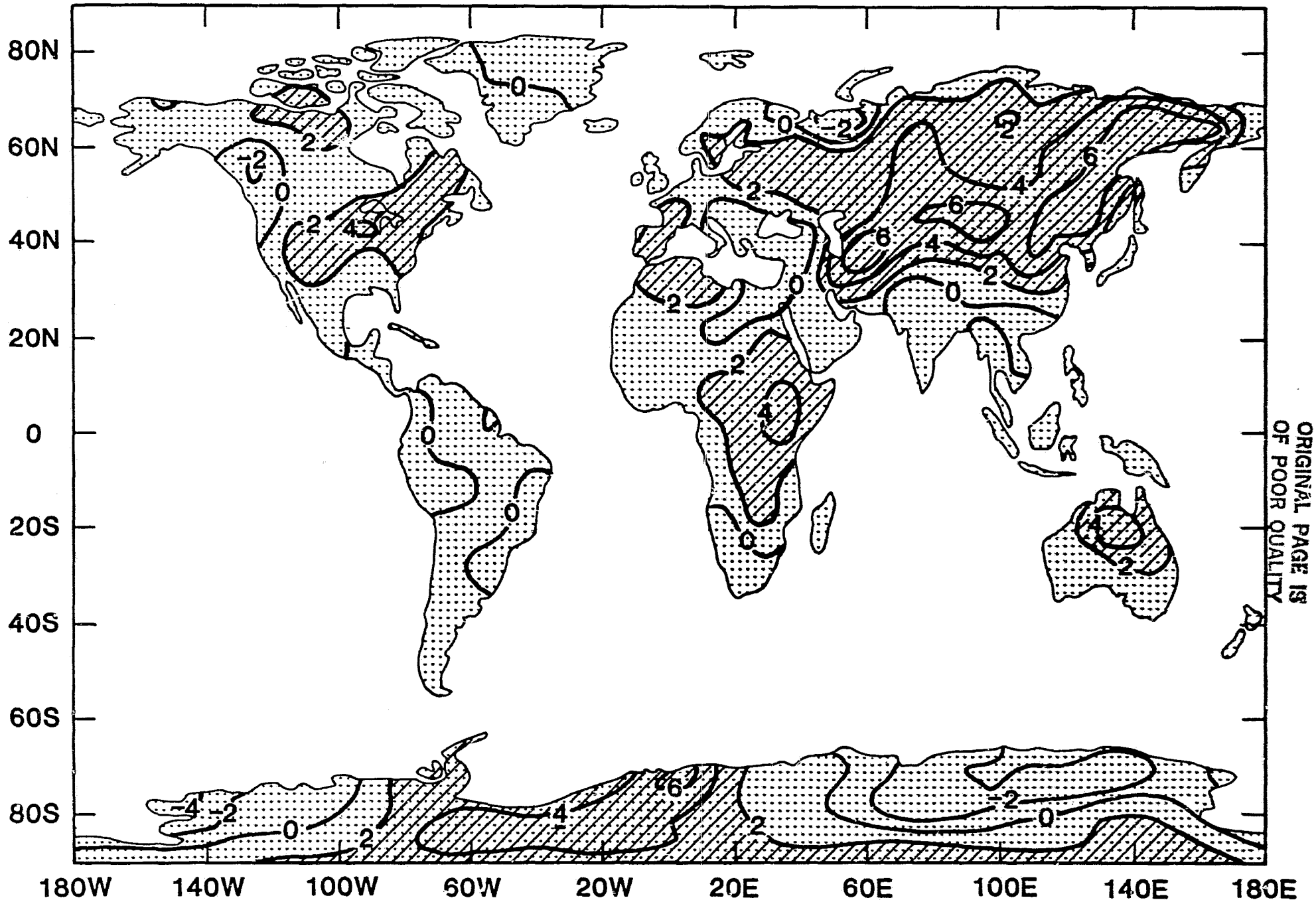
80N
60N
40N
20N
0
20S
40S
60S
80S
180W
140W
100W
60W
20W
20E
60E
100E
140E
180E
ORIGINAL PAGE IS
OF POOR QUALITY

Figure 12

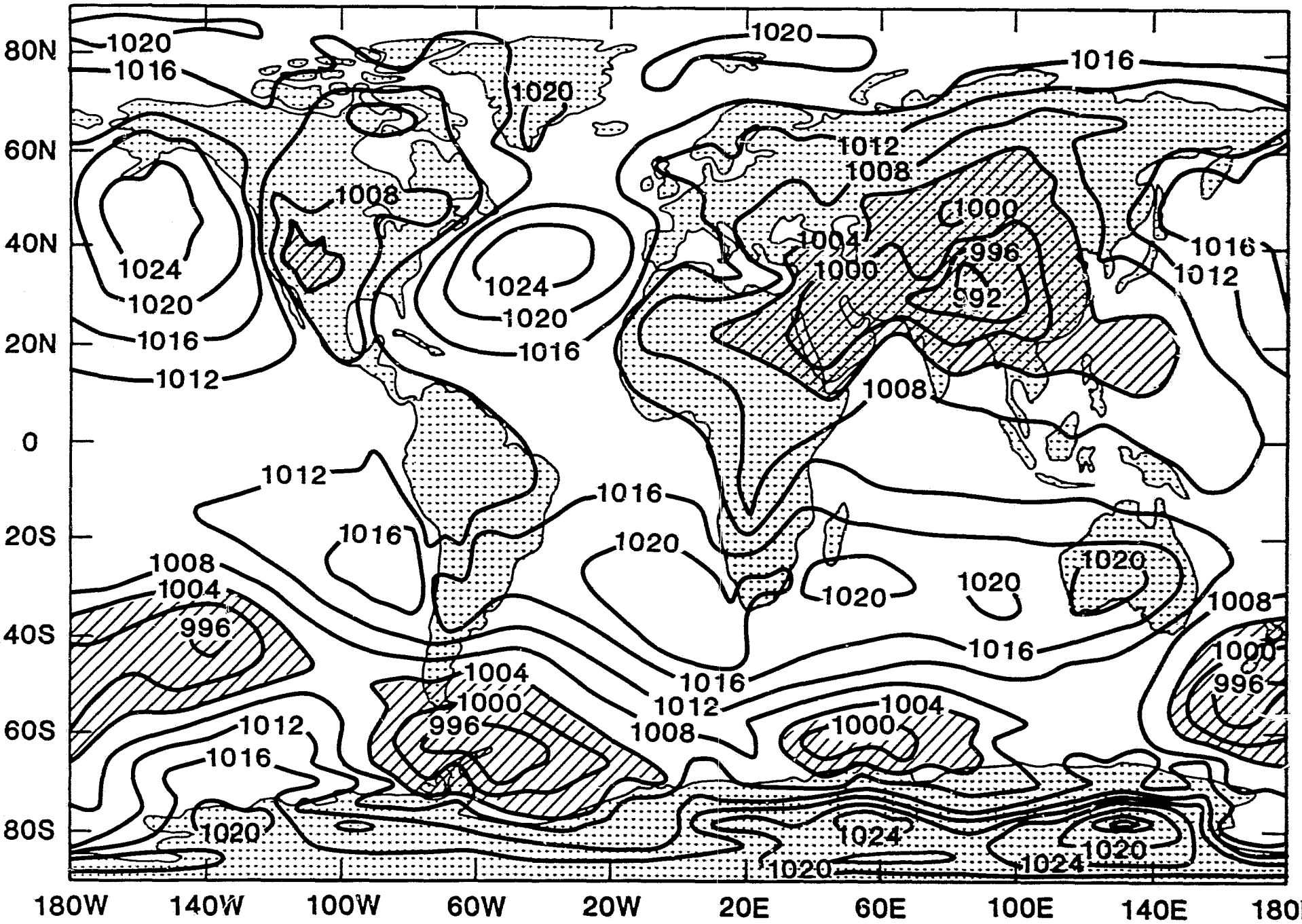

ORIGINAL PAGE IS
OF POOR QUALITY

Figure 13a

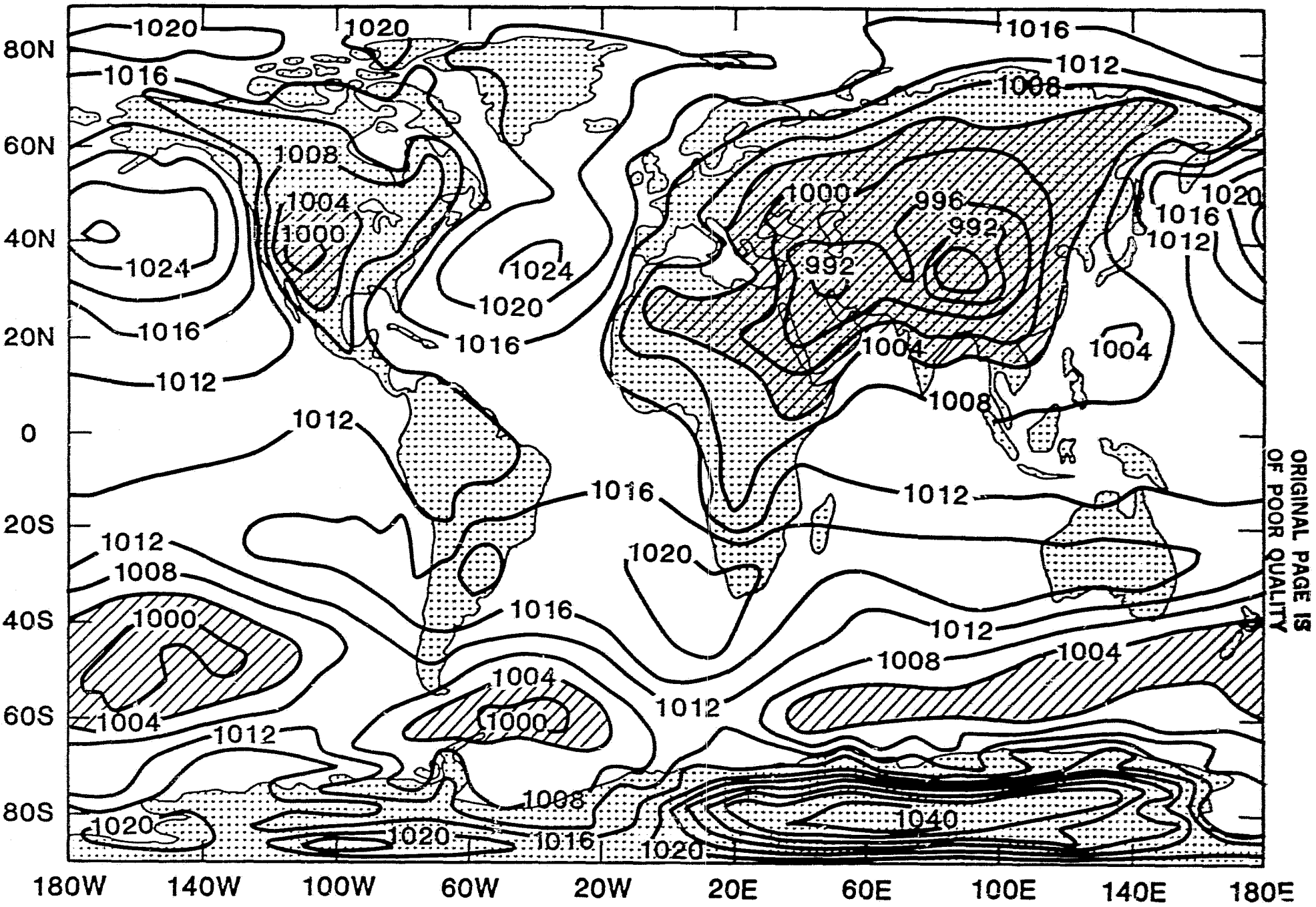
80N
60N
40N
20N
0
20S
40S
60S
80S
180W
140W
100W
60W
20W
20E
60E
100E
140E
180E
1020
1016
1012
1008
1004
1000
996
992
1024
1040
ORIGINAL PAGE IS
OF POOR QUALITY

Figure 13b

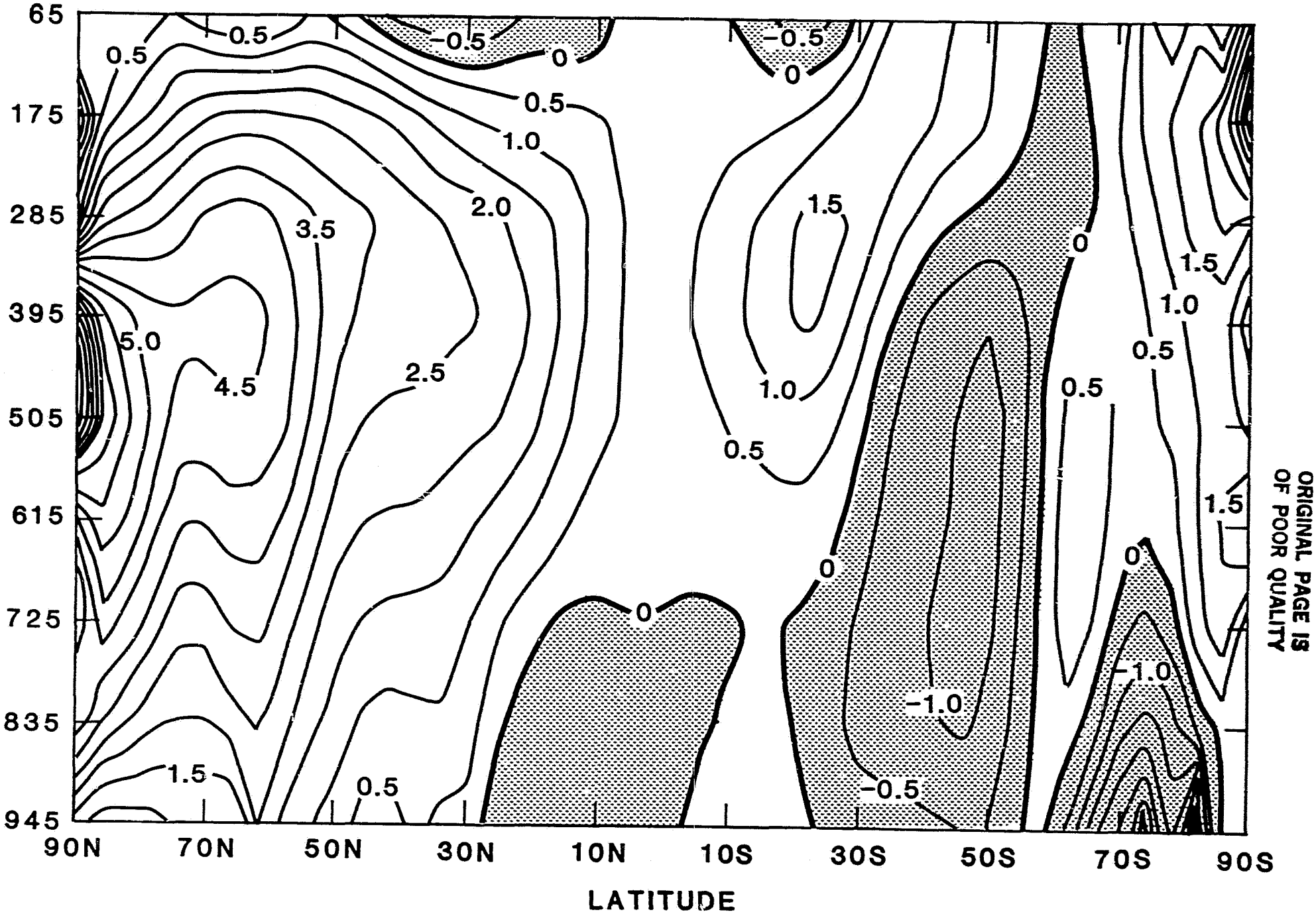
65
175
285
395
505
615
725
835
945
90N
70N
50N
30N
10N
10S
30S
50S
70S
90S
LATITUDE
0.5
-0.5
0
1.0
2.0
3.5
5.0
4.5
2.5
1.5
-1.0
ORIGINAL PAGE IS
OF POOR QUALITY

Figure 14

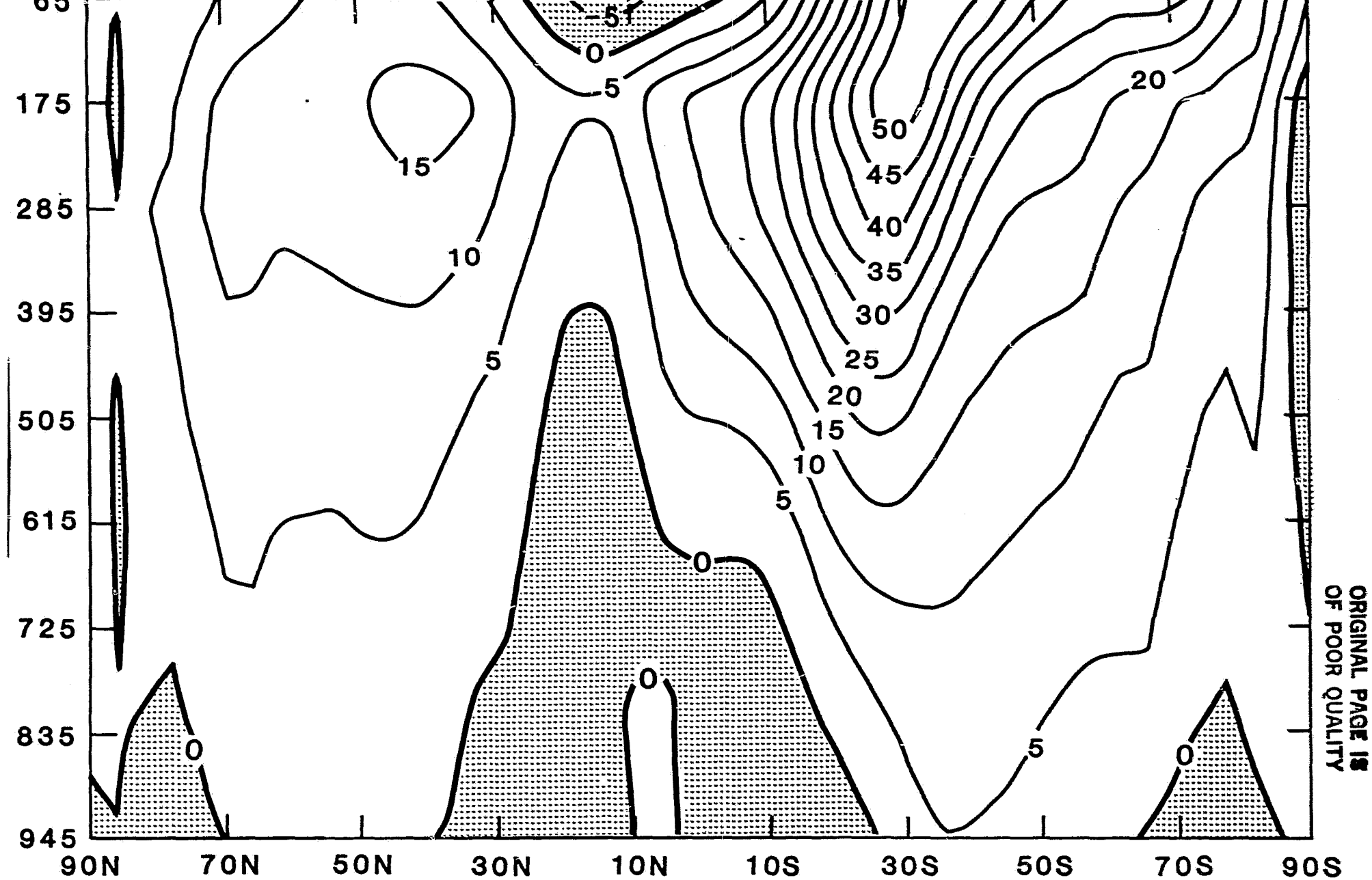

Figure 15a

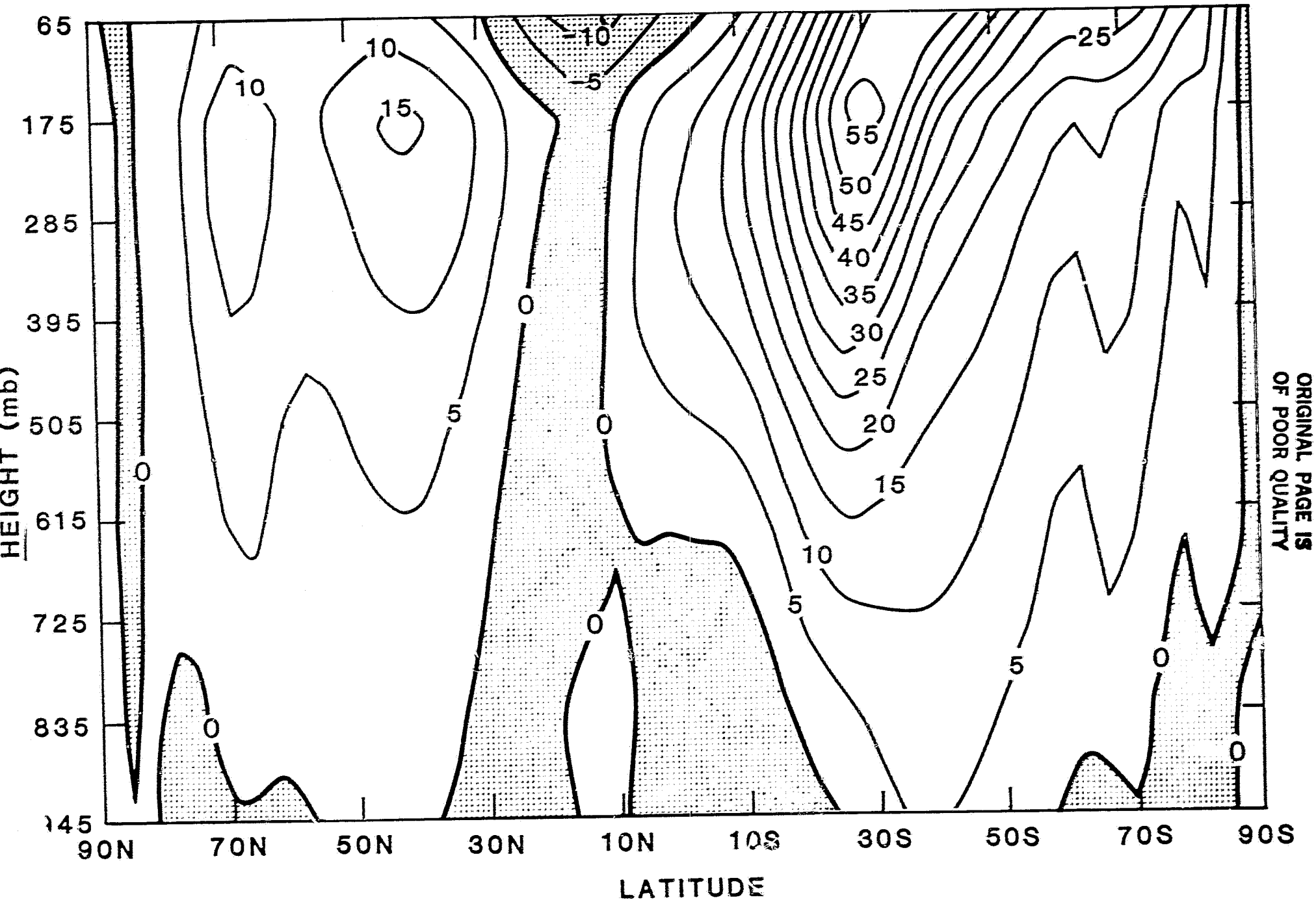
65
175
285
395
505
615
725
835
945
HEIGHT (mb)
90N
70N
50N
30N
10N
10S
30S
50S
70S
90S
LATITUDE
ORIGINAL PAGE IS
OF POOR QUALITY

Figure 15b

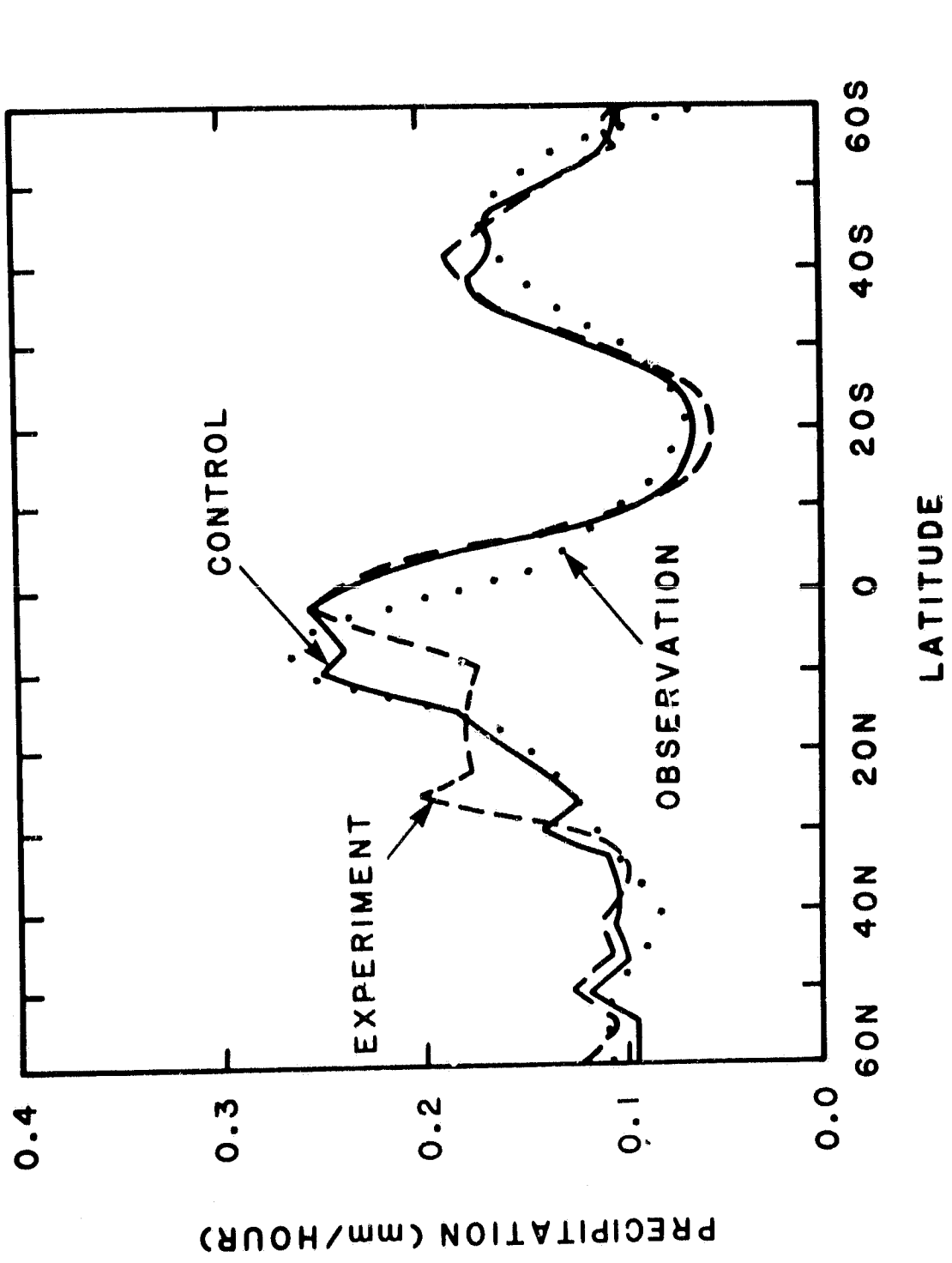

Figure 16

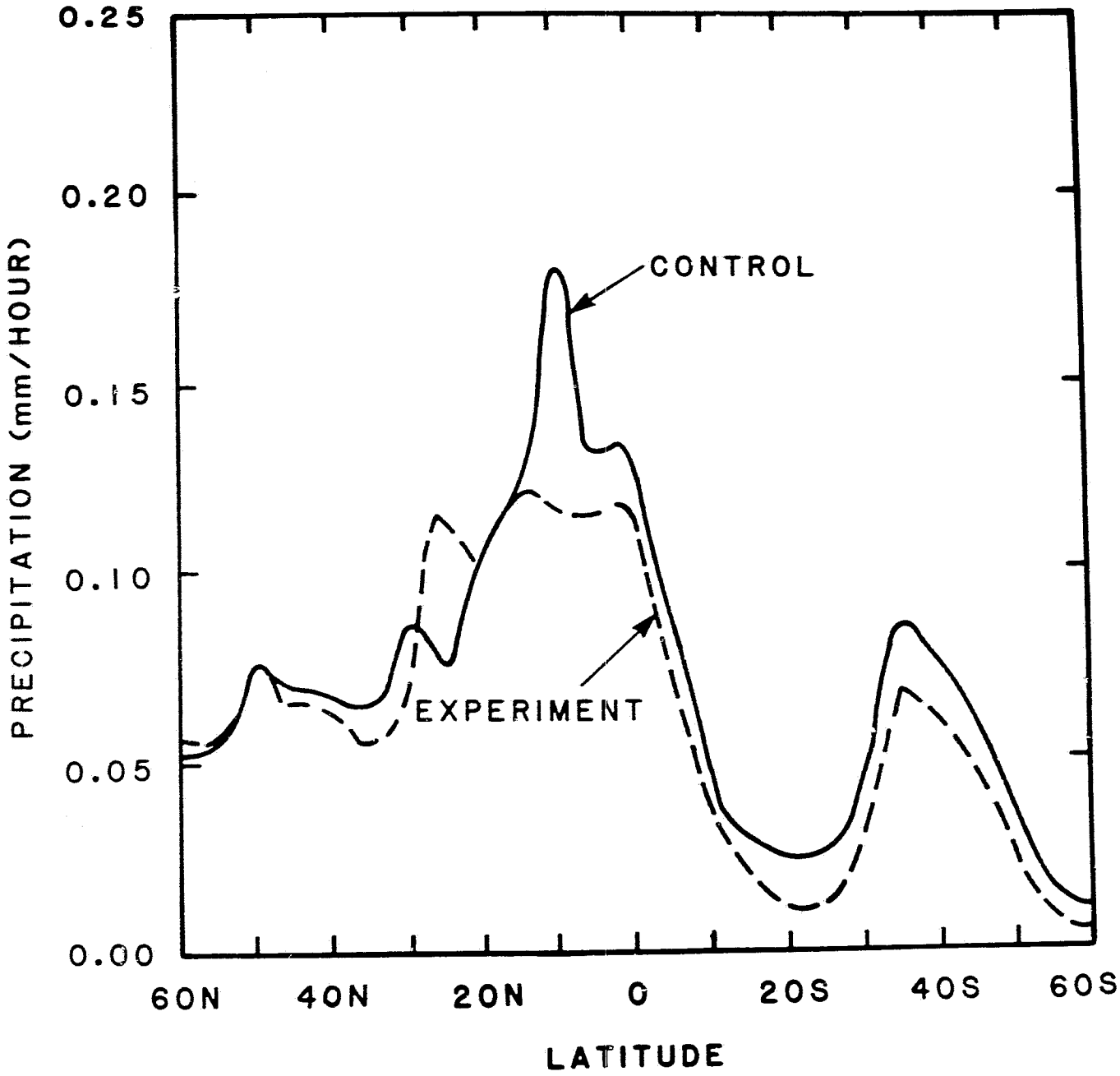

Figure 17